Fault-Tolerant Control for a High Altitude Long Endurance Aircraft

Christian Weiser * **Daniel Ossmann** **

* *German Aerosapce Center DLR, Münchener Str. 20, 82234 Weßling, Germany (e-mail: christian.weiser@dlr.de)*
** *Munich University of Applied Sciences HM, Lothstr. 64, 80335 Munich, Germany (e-mail: daniel.ossmann@hm.edu)*

Abstract: High Altitude Long Endurance (HALE) aircraft consist of extremely light-weight structures in combination with a high wingspan and high aspect ratio. The combination of these properties results in an unique dynamic behavior of the aircraft system featuring a strong interaction of structural and rigid body eigenmodes. These characteristics lead to specific demands on the robustness and fault tolerance of flight control algorithms of such aircraft. The control system must be able to navigate the aircraft safely along defined tracks even in case of fault scenarios. Due to the size of these aircraft they are usually over-actuated featuring multiple redundant control surfaces. This redundancy is used in this paper to design a fault tolerant control system ensuring optimal control performance during fault scenarios. The strategy is based on a fault detection and isolation (FDI) algorithm to detect malfunctioning control surfaces. This fault information is used to switch to alternate control laws in a multi-model control approach. The FDI filters are designed using the nullspace-based design paradigm, while the alternate controllers are synthesized applying structured H_∞ control design techniques.

Keywords: Fault Tolerance, Robust Control, Aircraft Control, Aircraft Operation.

1. INTRODUCTION

High Altitude Long Endurance (HALE) aircraft are designed to fly at altitudes of up to 25 km with satellite-like mission scenarios, requiring the platform to stay airborne for multiple days up to several months. These platforms shall be able to fly on a desired track and perform multiple cycles from takeoff to landing with the possibility of maintenance or exchange of the payload at relatively low cost. Staying airborne by the use of only solar energy demands extremely light weight aircraft structures. All these aspects result in a design with high structural flexibility, a low tolerance to external loads, an unusual low airspeed and a very small flight envelope compared to known unmanned aerial vehicles. Fig. 1 illustrates DLR's design of a HALE aircraft. The design of HALE platforms has been investigated for more than 20 years, e.g. Keidel (2000). First flights, as for example the NASA HELIOS (Noll et al. (2004)) as one of the most prominent examples, failed because they were very vulnerable due to atmospheric disturbances. But recent advances in solar cell and battery technology as well as composite structures allow a more feasible trade-off between structural weight, aspect ratio and flexibility of the structure. Although, several successful test flights took place with, e.g. the accident of the Zephyr in Wyndham, Australia Australian Transport Safety Bureau (ATSB) (2020), shows, that unexpected event like atmospheric disturbance can quickly lead to catastrophic failures. Thus, there is still a gap until the HALE aircraft technology will be reliable enough for a wide range of customers, which request guaranteed availability of e.g. surveillance or telecommunication services

Fig. 1. Illustration of DLR's High Altitude Long Endurance (HALE) Aircraft.

in the deployment region of the HALE aircraft. To close this gap, fault detection and diagnosis (FDD) as well as fault tolerant control (FTC) approaches are identified as techniques which need to be pragmatically pursued during the design of the HALE flight control system. This allows establishing a maximum degree of automation and enables close to optimal performance also in fault scenarios. In general, flight mechanical and aeroelastic analyses of a current HALE aircraft configuration investigated by Hasan et al. (2020); Voß et al. (2020) show, that the dynamics of this type of aircraft is very different from conventional UAVs in terms of eigenmodes and especially in an interaction of the structural dynamics with the short period mode. For this extraordinary type of aircraft, a specifically tailored flight control system was designed in Weiser and Ossmann (2022), which emphasizes robustness and disturbance rejection and thus requires lower performance specifications. Consequently, actuation failures in control surfaces related

to the lateral motion of the aircraft are much likely not to cause immediate system instability due to the large amount of robustness in the closed loop system. However, the control performance and accuracy may decrease drastically in a manner, which is not acceptable for navigation purposes anymore. To overcome this shortage, a multi-model control approach is chosen within this work which allows to specify backup controllers for the most common actuation failure scenarios enabling adequate performance also in case of faults.

2. MULTI-MODEL FAULT TOLERANT CONTROL DESIGN STRATEGY

The fault tolerant control strategy is based on a multi-model control approach. In the nominal case, i.e., no faults are present in the system, the nominal controller ensures optimal performance per design. If a fault occurs in the system, the fault detection and isolation module detects and isolates the fault using the known inputs u and measured outputs y of the system. These signals are processed through residual filters, a residual evaluation function and a decision-making logic providing the Boolean information vector ι. This vector indicates, which fault is active in the system. Via a supervisory logic, as illustrated in Fig. 2, a switching signal σ is processed to the reconfigurable control system. The multi-model control system, schematically illustrated in Fig. 3, consists, beside the nominal controller, of a number of backup controllers, each designed for a distinct fault scenario. Depending on the isolated fault scenario, the corresponding backup controller is activated. Each controller is designed based on a dedicated linearized model of the aircraft dynamics.

Each multi-input multi-output controller within the multi-model control design approach is designed by optimization. The optimization process for the gains of the fixed structure control system follows the constrained min/max optimization procedure proposed by, e.g., Joos et al. (2002), where the generic controller gains are tuned as

$$\begin{aligned} \min_{K} \quad \max_{i} \quad & f_i(K), \\ \text{s.t.} \quad & g_j(K) < 1 \\ & K_{\min} < K < K_{\max} \end{aligned} \tag{1}$$

where $f_i(K)$ are the $i = 1, \ldots, n_s$ posed soft requirements, and $g_j(K)$ are the $j = 1, \ldots, n_h$ hard requirements. The controller gains are stacked in the vector K and are limited by the upper and lower bounds $K_{\min}$ and $K_{\max}$. The software normalizes the soft and hard constraints and applies non-smooth optimization techniques to solve

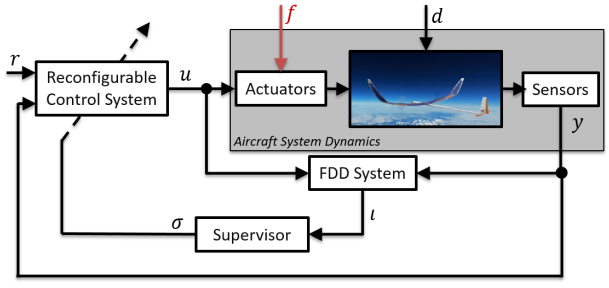

Fig. 2. Overall system interconnections including FDD-, control- and supervisory-system, and aircraft system dynamics.

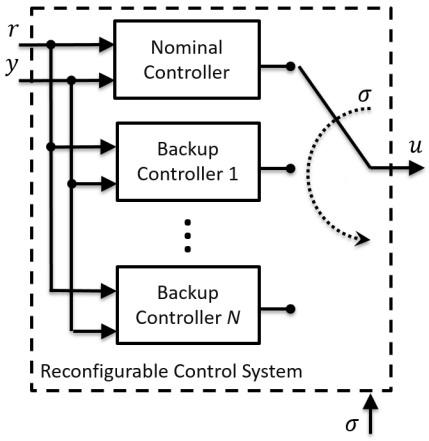

Fig. 3. Illustration of the reconfigurable multi-model control system.

the corresponding multi-objective problem as presented in Apkarian et al. (2015); Apkarian and Noll (2006). The soft and hard design requirements f and g in (1) are based on classical control objectives, e.g., desired margins, disturbance rejection, overshoot, tracking or maximum gains and desired loop shapes. Time-domain criteria can be formalized as desired responses to *step reference signals* or *disturbance signals* in terms of response times and steady state errors. Equivalently, the desired bandwidth of the closed loop can be defined as frequency domain criteria. Additionally, phase and gain *margins* can be used as criteria to improve the robustness. More details on the actual criteria used for each cascaded control loop are provided in section 4. Note that this approach can be easily extended to a parameter dependent control design in case a larger part of the flight envelope needs to be considered, as presented in Ossmann et al. (2019).

3. FDI SYSTEM DESIGN APPROACH

The FDI system basically consists of a linear residual filter, which provides residual signals allowing to detect and isolate the considered additive faults, the residual evaluation post-processing the residual signals, and finally the decision making, providing the Boolean information if a fault is present or not in the system.

3.1 Fault Detection filter design

A linear residual generator processes the measurable system outputs $y(t)$ and inputs $u(t)$ to generate the residual signals $r(t)$, which serve for decision making on the presence or absence of faults. Commonly, around an equilibrium point a linearized additive fault model can be described by the input-output form

$$y(s) = G_u(s)\mathbf{u}(s) + G_d(s)\mathbf{d}(s) + G_f(s)\mathbf{f}(s), \tag{2}$$

where $\mathbf{y}(s)$, $\mathbf{u}(s)$, $\mathbf{d}(s)$ and $\mathbf{f}(s)$ are Laplace-transformed vectors of the p-dimensional system output vector $y(t)$, m_u-dimensional disturbance input vector $u(t)$, m_d-dimensional input vector $d(t)$ and m_f-dimensional fault input vector $f(t)$. $G_u(s)$, $G_d(s)$ and $G_f(s)$ are the transfer function matrices from the control inputs to outputs, disturbance inputs to outputs and fault inputs to outputs,

respectively. The input-output form of a residual generator for this system is given by

$$\mathbf{r}(s) = Q(s) \begin{bmatrix} \mathbf{y}(s) \\ \mathbf{u}(s) \end{bmatrix}. \tag{3}$$

The internal form of the residual generation system, obtained by replacing $\mathbf{y}(s)$ in (3) by its expression in (2), is given by

$$\mathbf{r}(s) = R_u(s)\mathbf{u}(s) + R_d(s)\mathbf{d}(s) + R_f(s)\mathbf{f}(s)\,, \tag{4}$$

where

$$[\,R_u(s)\,|\,R_d(s)\,|\,R_f(s)\,] := Q(s)G_e(s) \tag{5}$$

with

$$G_e(s) := \left[\begin{array}{c|c|c} G_u(s) & G_d(s) & G_f(s) \\ I & 0 & 0 \end{array}\right]. \tag{6}$$

The choice of $Q(s)$ needs to guarantee decoupling of all control- and disturbance inputs from the residual signal, i.e.

$$Q(s) \begin{bmatrix} G_u(s) & G_d(s) \\ I & 0 \end{bmatrix} = 0. \tag{7}$$

To actually allow for the detection and isolation of the faults, the faults need to be coupled to the residual, i.e.,

$$Q(s) \begin{bmatrix} G_{f,i}(s) \\ 0 \end{bmatrix} \neq 0, \tag{8}$$

for $i = 1 \ldots m_f$. Thus, each fault f_i needs to be somehow coupled with the residual r. As additional design constraint the residual filter $Q(s)$ needs to be *stable* in order to bound the residual in case of bounded input signals, *proper* to provide a physically realizable filter, and guarantee $R_f(0) \neq 0$ to have a steady state effect from $f(t)$ to $r(t)$ in case of constant faults, see Varga (2017). This rather generic formulation of the fault detection problem is a widely studied topic in literature. Methods and its applications based on parity spaces (Patton and Chen (1994)), on Kalman filters (Efimov et al. (2011); Berdjag et al. (2013)), on H_∞ (Marcos (2011)) as well as linear parameter varying methods (Vanek et al. (2014)) or nullspace methods (Varga (2007, 2017)) among others are available. In this paper we rely on the nullspace method as it directly tackles to solve the decoupling problem (7) directly while considering (8) together with the stability constraint. Numerically sophisticated tools are available and presented in detail in Varga (2017).

3.2 Fault Isolation Extension

Fault detection is the process of detecting any fault in the system. Following (8), considering multiple faults in a system, fault detection may be achieved by a single residual r, in case all faults are coupled with the scalar residual. This, however, is usually not sufficient for technical processes and especially not for safety critical systems like aircraft. Such systems cannot be simply switched-off in case of faults. Thus, faults need to be detected and clearly localized (i.e., isolated), enabling dedicated counteractions to the faults as hard- or software reconfiguration. Full fault isolation for a system is given, if for each fault $i = 1, \ldots, m_f$ a unique residual can be generated, which is only activated by one fault. Physically, this requires an over-actuated and over-sensed system, i.e., providing enough open-loop control inputs and measurement output to enable a complete decoupling of each residual from all disturbances and all but one fault. HALE aircraft, however, provide such system configurations and thereby enable full fault isolation. A method has been provided in Varga (2009) which allows to determine all possible fault to residual signatures before the actual residual filter design. This check is used within the presented work. If full fault isolation is possible, the decoupling condition in (7) can be extended by all faults, which need to be decoupled from the residual. In other words, all faults but one are considered as disturbances during the residual filter design. For m_f faults, the design is repeated m_f times to generate $N = m_f$ residual generators, each of them being prone to a single fault. By maintaining the coupling condition (8)

$$Q(s) \begin{bmatrix} G_{f,i}(s) \\ 0 \end{bmatrix} \neq 0, \text{ for } i = 1, \ldots, m_f$$

and extending the decoupling condition with the faults to be decoupled from the residual

$$Q(s) \begin{bmatrix} G_u(s) & G_d(s) & G_{f,j}(s) \\ I & 0 & 0 \end{bmatrix} = 0, \text{ for } j \neq i. \tag{9}$$

The design process is repeated N times. These N filters provide distinct residual signals solving the fault detection and isolation problem.

3.3 Residual evaluation and decision making

To decrease the sensitivity of the FDD system in the fault free case, it is often favorable to evaluate each residual signal over a certain period of time. This evaluation of the residual signal requires the computation of a measure of the residual signal energy, for which the 2-norm of the signal is usually an appropriate choice. The Narendra signal evaluation scheme as an approximation of the 2-norm in the form

$$\theta_i(t) = \alpha_i |r_i(t)| + \beta_i \int_0^t e^{-\gamma_i (t-\tau)} |r_i(\tau)| d\tau, \tag{10}$$

with $i = 1 \ldots N$, can be applied for each residual r_i. The filter parameters $\alpha_i \geq 0$ and $\beta_i \geq 0$ represent weights for instantaneous and long-term values, respectively, and $\gamma_i > 0$ is the forgetting factor. The evaluation signal $\theta_i(t)$ is compared to a specific threshold $\tau_{i,th}$ in the decision making process to determine the decision signal ι_i using the decision logic

$$\begin{array}{l} \theta_i(t) < \tau_{i,th} \;\Rightarrow\; \iota_i(t) = 0 \;\Rightarrow\; \text{no fault} \\ \theta_i(t) \geq \tau_{i,th} \;\Rightarrow\; \iota_i(t) = 1 \;\Rightarrow\; \text{fault.} \end{array} \tag{11}$$

The appropriate selection of the values of the free parameters α_i, β_i or γ_i, with an appropriate threshold $\tau_{i,th}$ essentially influences the performance of the FDD system. The supervisory algorithm evaluates the decision vector $\iota = [\iota_1, \ldots, \iota_N]^{\mathrm{T}}$. Depending on the identified fault scenario, the supervisory system actives the backup controller via the variable σ (Fig. 3). For smooth transition between the nominal and backup controller, a 2 s blending phase between the controller output signals is intended upon a change in σ.

4. FAULT TOLERANT SYSTEM DESIGN FOR DLR'S HALE AIRCRAFT

As an example of a HALE aircraft configuration, the DLR HALE aircraft is used (Nikodem and Bierig (2020)). A graphical representation of the aircraft is depicted in Fig. 1. The considered configuration is designed for flight

in altitudes of up to 20 km and has a takeoff mass of about 135 kg in combination with wingspan of about 27 m. The aircraft is controlled by an elevator, four ailerons (inner/outer aileron on each wing), which are actuated separately, and a single rudder. The aircraft is propelled by two electric engines with constant pitch propellers, which are powered by solar cells and a battery system used as buffer. Note that all ailerons are actuated with the same commanded signal, only altered by the sign on the left and right side. This basic control allocation is justified as the inner aileron pair has low effectiveness due to its lever arm, while the span-wise position of the outer aileron pair is also limited due to possible flutter as well as aileron reversal caused by aeroelastic effects. Thus, for the control synthesis in lateral axis, the aileron signals are simply fed to both aileron pairs simultaneously in order to achieve maximum roll acceleration.

4.1 Fault Scenarios

For navigation, the control of the lateral motion is crucial, allowing to navigate on a predefined ground track. The lateral motion is controlled via the single rudder and two aileron pairs. Electro-mechanical actuators (EMAs) are installed for steering these control surfaces. The redundancy on the ailerons can be exploited in case one or more ailerons are lost by using a fault tolerant control scheme presented herein. EMAs are most prone to jamming and runaway faults, see Ossmann and van der Linden (2015); Romeral et al. (2010). Thus, the considered fault herein is a slow runaway of the actuator induced by sensor faults in the actuators' control loops. Due to the chosen model-based method, the presented approach is expected to work as well for jamming scenario. Note that only single fault scenarios are considered. In case of multiple, simultaneous aileron faults, additional backup controllers need to be designed.

4.2 Control System Design

The control system architecture, which was designed in Weiser and Ossmann (2022) is depicted in Fig. 4 and consists of a conventional cascaded control architecture. As shown in the figure, it includes envelope protections based on the angle of attack α, the pitch angle θ, and the calibrated airspeed V_{cas}. The core element is the attitude control system providing aileron ξ, elevator η and rudder deflection ζ to the aircraft. Thus, the attitude controller is responsible for following bank attitude, pitch attitude, and lateral load factor commands (ϕ, θ, n_y) given by the

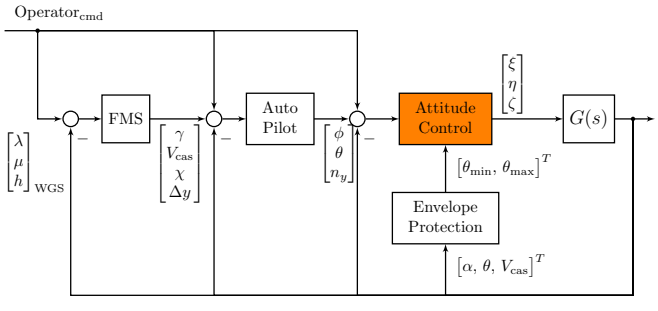

Fig. 4. Baseline Flight Control System.

Table 1. Roll attitude and turn coordination controller tuning specifications.

Specification	Acceptable Value	Frequency Region
Roll att. bandwidth(BW)	2 rad/s	-
Turn coord. BW	2 rad/s	-
Gain/Phase Margin	6 dB/45 deg	[0; 4] rad/s
Gain/Phase Margin	8 dB/60 deg	]4; inf[rad/s
Desired control bandwidth	4 rad/s	

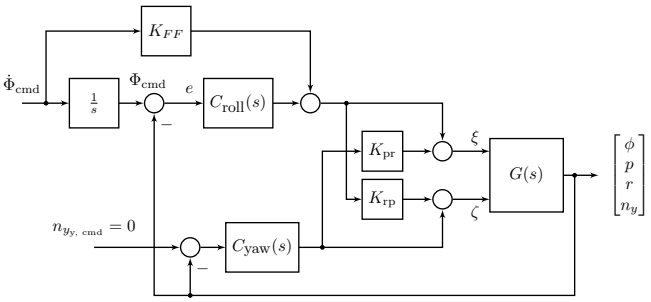

Fig. 5. Inner Loop lateral axis RCAH control structure.

autopilot. This module is the critical part of the flight control system in case of an actuator failure and thus is described in more detail. The autopilot receives the flight path angle γ, the calibrated airspeed, the heading χ and lateral offset from the trajectory Δy. The operator provides either 3D way points (λ, μ, h) to the flight management system, a flight path vector (V, γ, χ) or gives direct input to the attitude controller.

Table 1 lists the desired controller specifications for the fixed structure control system tuning. The stability and performance requirements are derived from handbooks SAE International (2012) and can also be found in literature dealing with similar systems, e.g. Köthe (2019). For optimization of the lateral controllers (nominal as well as backup), the fixed control structure depicted in Fig. 5 is used. The structure was derived following an analysis of the open loop system, which revealed a very strong coupling between yaw and roll motion, which led to the decision to introduce the cross-feed gains K_{rp} and K_{pr} and a combined tuning of the roll and yaw axis. For the exemplary controller developed herein, the optimization process has been executed five times for five different scenarios:

- nominal controller: all control surfaces in operation
- four backup controllers: design with one of the four ailerons not available

4.3 FDI System Design

Based on the methodology described in Section 3 four residual filters are designed. Each of those filters generates a residual, which is excited by a single fault on one of the aileron actuators, while it is decoupled from the other three. For the residual filter design the aero-elastic linear model of the HALE aircraft, generated at a trim point at 9 m/s at sea-level, is reduced from 72 states to 14 states, mainly covering the aircraft's rigid body dynamics. To avoid any influence of the higher modes on the residual via the measured outputs, the desired poles of the residual filter are placed at -1. This ensures a roll-off at about

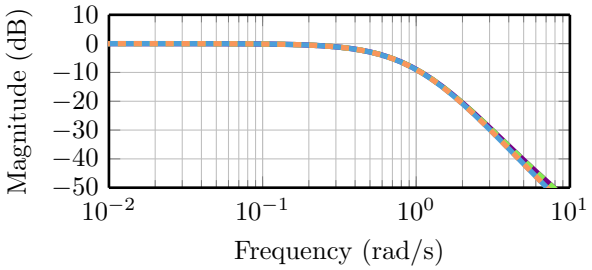

Fig. 6. Bode-magnitude plot of the four fault-to-residual transfer functions systems.

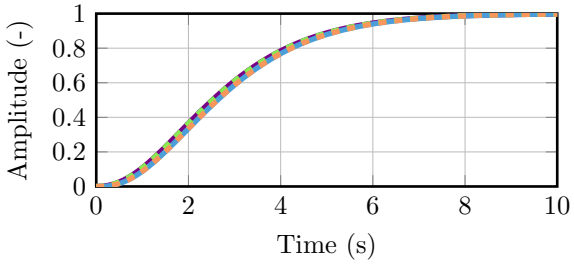

Fig. 7. Step-response plots of the four faults to their coupled residuals.

1 rad/s in the faults-to-residuals transfer functions. Fig. 6 depicts the Bode magnitude plot from a fault on the inner left aileron to the first residual (——), from a fault on the outer left aileron to the second residual (——), from a fault on the inner right aileron to the third residual (- - -), and from a fault on the outer right aileron to the fourth residual (- - -). Fig. 7 shows the accordant step responses of these channels, where the figure follows the same color coding as Fig. 6. In each of the two figures two lines exactly overlay each other twice. This is due to the symmetric dynamical characteristics of the lateral motion of the aircraft. It further shows that the residual filter design algorithm is able to maintain these properties so that the fault-to-residuals dynamics are exactly the same in case of each aileron pair. The chosen dynamics allow filtering out high frequency noise as well as the influence of the high frequency modes of the aircraft system. Still, the residual filters show fast enough dynamics to detect the relevant fault. Slow runaways as well as a stuck actuator faults excite the residuals at a low frequencies. For the runaway fault explicitly considered herein the relevant frequency range is determined by the actual runaway rate of the fault. The required bandwidth is proportional to the defined maximum runaway rate to be considered.

4.4 Closed loop simulation results

For control system validation purposes, an actuator runaway of the right outer aileron is simulated with a high-fidelity non-linear simulation model. The non-linear model aircraft consists of a vortex-lattice aerodynamic model coupled with a linear structural model as presented in Weiser and Ossmann (2022) The simulations are performed with the nominal controller as well as with the FDI logic triggering the activation of the backup controller. Compared to the demanded roll control input at 5 s of the simulation scenario, the actuator runaway, activated at 1 s simulation time, induces a roll motion in the adverse

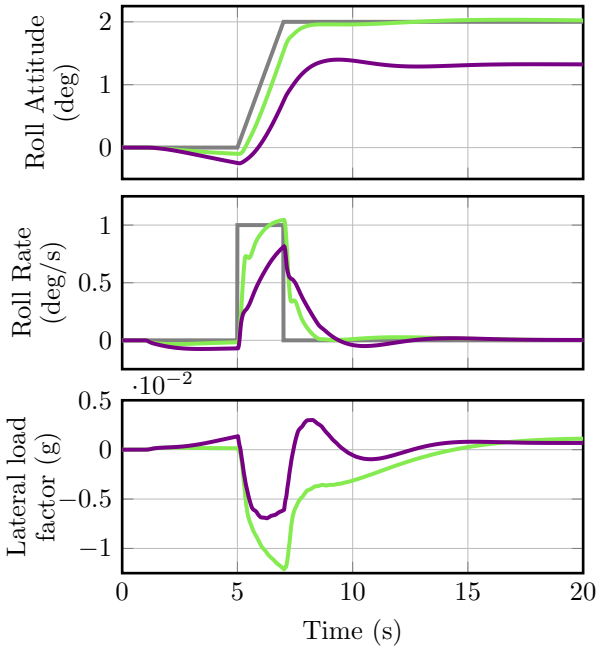

Fig. 8. System variables for the nominal (——) and backup (——) controller during a 2 deg/s right outer aileron runaway during a roll command input (——).

direction. This shall reflect a bad case situation, in which the fault does support the desired motion of the aircraft. Relevant aircraft states are shown in Fig. 8. The fault detection and isolation occurs right away due to the dominance of the runaway fault in the corresponding residual signal. Fig. 8 shows in the first diagram that in case of the reconfiguration the roll attitude can still be tracked in reasonable time. The integrator in the controller ensures the roll attitude tracking also in case of the fault. However, it takes minutes to recover the fault effect (not visible in the first diagram). In the second diagram, it can be seen that a higher roll rate is ensured by the backup controller, while also the lateral acceleration is higher. This is acceptable,

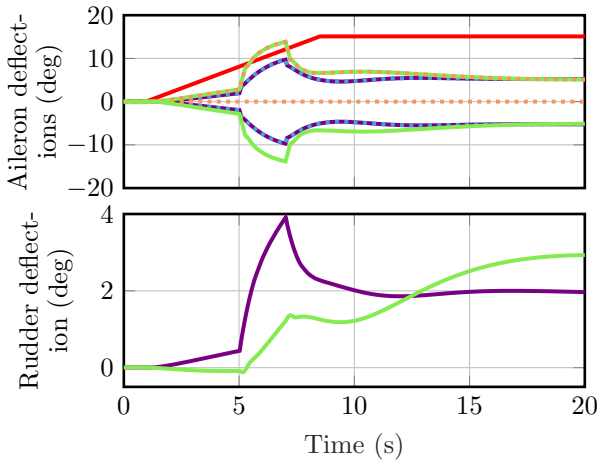

Fig. 9. Control commands of the nominal (——,·····) and backup (——,·····) controller for the 4 ailerons (upper diagram) and the rudder (lower diagram) during a 2 deg/s runaway of the right outer aileron (——) and a roll command input.

as the lateral load factor limit for maneuvering was set to a value of 0.03 g, see SAE International (2012).

Moreover, it can be seen that the use of the commanded rudder deflection is only 50% compared to the nominal case, where the nominal controller tries to compensate the fault scenario via the rudder, visible in the second diagram of Fig. 9. Such an extensive use of the rudder is not favorable due to structural constraints. In case of the backup controller, the aileron commands are increased instead to accommodate the fault, while the rudder deflections remains lower as well as slower. The first diagram of Fig. 9 compares the aileron commands of the two controllers in the fault scenario. The backup controller compensates the faulty aileron via larger commands on the remaining ailerons, while keeping the command signal of the faulty aileron at zero (—,·····). The nominal controller provides symmetric commands (—,·····) to the aileron pairs, although one aileron is running away, illustrated via the actual position of the faulty aileron position (—).

5. CONCLUSION

In this paper the design of a fault tolerant flight control system for a high altitude long endurance aircraft has been presented. A classical cascaded flight controller structure is developed, which is tuned based on non-linear optimization techniques to for dedicated fault scenarios of the the aircraft's ailerons. The multi-model-based controller designs have been verified using a high fidelity non-linear simulator of the HALE aircraft, confirming the functionally of the developed approach.

ACKNOWLEDGEMENTS

The presented work is part of the German Aerospace Center's High Altitude Platform (HAP) project. Methods herein are developed based on the project's requirements and data.

REFERENCES

Apkarian, P. and Noll, D. (2006). Nonsmooth H_∞ Synthesis. *IEEE Transactions on Automatic Control*, 51(1), 71–86.

Apkarian, P., Dao, M., and Noll, D. (2015). Parametric robust structured control design. *IEEE Transactions on Automatic Control*, 60, 1857–1869.

Australian Transport Safety Bureau (ATSB) (2020). In-flight break-up involving airbus zephyr unmanned aerial vehicle. Technical report.

Berdjag, D., Cieslak, J., and Zolghadri, A. (2013). *Fault Detection and Isolation of aircraft air data/inertial system*, chapter Fault Detection and Isolation of aircraft air data/inertial system, 317–332. Torus Press.

Efimov, D., Zolghadri, A., and Simon, P. (2011). Fault detection improving by extended Kalman filter adjustment for oscillatory failure case in aircrafts. In *Proc. of 4th European Conference for Aerospace Sciences*. St. Petersburg, Russia.

Hasan, Y.J., Roeser, M.S., Hepperle, M., Niemann, S., Voß, A., Handojo, V., and Weiser, C. (2020). Flight mechanical design and analysis of a solar-powered high-altitude platform. In *69. Deutscher Luft- und Raumfahrtkongress*.

Joos, H.D., Bals, J., Looye, G., Schnepper, K., and Varga, A. (2002). A multi-objective optimisation-based software environment for control systems design. In *IEEE International Conference on Control Applications and International Symposium on Computer Aided Control Systems Design*, 7–14.

Keidel, B. (2000). *Auslegung und Simulation von hochfliegenden, dauerhaft stationierbaren Solardrohnen*. Ph.D. thesis, TU München.

Köthe, A. (2019). *Flight Mechanics and Flight Control for a Multibody Aircraft*. Ph.D. thesis, Technische Universität Berlin.

Marcos, A. (2011). Application of H-infinity fault diagnosis to ADDSAFE benchmark: the control surface jamming case. In *Proc. of AIAA Guidance, Navigation and Control Conference*. Portland, Oregon, USA.

Nikodem, F. and Bierig, A. (2020). Dlr hap - herausforderungen in der entwicklung der höhenplattform und ihrer anwendungen. In *Deutscher Luft- und Raumfahrtkongress*.

Noll, T.E., Brown, J.M., Perez-Davis, M.E., Ishmael, S.D., Tiffany, G.C., and Gaier, M. (2004). Investigation of the helios prototype aircraft mishap. techreport, NASA.

Ossmann, D., Luspay, T., and Vanek, B. (2019). Baseline flight control system design for an unmanned flutter demonstrator. In *2019 IEEE Aerospace Conference*.

Ossmann, D. and van der Linden, F. (2015). Advanced sensor fault detection and isolation for electromechanical flight actuators. In *2015 NASA/ESA Conference on Adaptive Hardware and Systems*.

Patton, R.J. and Chen, J. (1994). Review of parity space approaches to fault diagnosis for aerospace systems. *Journal of Guidance, Control, and Dynamics*, 17(2), 278–285.

Romeral, L., Rosero, J., Espinosa, A.G., Cusido, J., and Ortega, J. (2010). Electrical monitoring for fault detection in an ema. *IEEE Aaerospace and Electronic Systems Magazine*, 25, 4–9.

SAE International (2012). ARP94910 Vehicle Management Systems - Specification Guide for Flight Control Design, Installation and Test of Military Unmanned Aircraft. Technical report.

Vanek, B., Edelmayer, A., Szabo, Z., and Bokor, J. (2014). Bridging the gap between theory and practice in LPV fault detection for flight control actuators. *Control Engineering Practice*, 31, 171–182.

Varga, A. (2007). On designing least order residual generators for fault detection and isolation. In *Proc. of 16th International Conference on Control Systems and Computer Science*, 323–330. Bucharest, Romania.

Varga, A. (2017). *Solving Fault Diagnosis Problems - Linear Synthesis Techniques*. Springer International Publishing.

Varga, A. (2009). On computing achievable fault signatures. *IFAC Proceedings Volumes*, 42(8), 935–940.

Voß, A., Handojo, V., Weiser, C., and Niemann, S. (2020). Preparation of loads and aeroelastic analyses of a high altitude, long endurance, solar electric aircraft. In *Aerospace Europe Conference*.

Weiser, C. and Ossmann, D. (2022). Baseline flight control system for high altitude long endurance aircraft. In *AIAA SCITECH 2022 Forum*. American Institute of Aeronautics and Astronautics.